Diffusion of DNA in Nanoslits

Elizabeth A. Strychalski,*,†,§ Stephen L. Levy,‡,§ and Harold G. Craighead‡

Department of Physics, and School of Applied and Engineering Physics, Cornell University, Ithaca, New York 14853

Received June 10, 2008; Revised Manuscript Received August 14, 2008

ABSTRACT: We observed the free diffusion of individual 10 kbp, (1/2)λ (24.2 kbp), and λ (48.5 kbp) double-stranded deoxyribonucleic acid (DNA) molecules in fused-silica nanoslits with depths from 541 to 24 nm using epifluorescence video microscopy. Diffusivity, D, scaled with nanoslit depth, h, according to $D \propto h^{\alpha}$, where α was 0.47 ± 0.05, 0.51 ± 0.06, and 0.47 ± 0.05 for 10 kbp, (1/2)λ, and λ DNA, respectively, in disagreement with the value of two-thirds predicted by blob theory. We observed no change in scaling behavior for h less than the persistence length of DNA, as predicted by reflecting rod theory. The scaling of D with DNA length, N, followed $D \propto N^{-1}$, indicating hydrodynamic screening in accordance with Rouse dynamics. Our results establish these scaling exponents for smaller h and greater DNA confinement than previous studies.

1. Introduction

Nanoslits, nanofluidic channels with depths much smaller than widths, have received considerable attention in recent experimental and theoretical research. Observing highly confined DNA molecules in nanoslits can further fundamental polymer physics, give insight into the behavior of confined DNA in biological systems, and guide the development of new methods for manipulating and analyzing DNA and other biologically relevant molecules using fluidic platforms. Many fluidic devices have incorporated nanoslits as critical elements for interrogating various biological molecules,[1−13] and the development of new nanofluidic devices for biomolecular analysis can benefit from studies of the conformation and dynamic behavior of highly confined polymers. For example, the optimization of nanofluidic devices for biomolecular separations, such as long nanoslits,[6,11] requires an understanding of confined analyte diffusion to predict band broadening.

Confinement dramatically alters both the static and dynamic behavior of an individual, isolated polymer in good solvent. A polymer's steric interaction with the confining geometry results in an equilibrium conformation that differs from the bulk state and subsequently changes the polymer's dynamic properties, such as diffusion. A polymer may also interact with itself via hydrodynamic interactions, which arise from coupling between the movement of various polymer segments through the solvent velocity induced by their motion.[14] The length scale over which hydrodynamic interactions occur depends upon the confining geometry,[15] because the solvent velocity approaches zero at the boundaries (assuming a no-slip boundary condition[16]). Blob[15,17,18] and reflecting rod theories[19] have been proposed to describe polymers subject to various degrees of confinement. In order to test these theories and search for a crossover between their regimes of applicability in nanoslits, we investigated the effects of increased confinement on the free diffusion of DNA molecules of different lengths.

By studying the behavior of individual, confined DNA molecules in nanoslits, experiments and molecular simulations have attempted to verify the predictions of blob and reflecting rod theories. A thorough review of recent studies was provided by Hsieh et al.[10] As discussed below, both experimental and simulation results presented in the literature contain contradictory evaluations of blob theory's ability to accurately predict the scaling of polymer diffusivity, D, with the confining nanoslit depth, h. Additionally, several recent experimental results concerning nanoslits with depths on the order of the persistence length of double-stranded DNA (approximately 50 nm[20]) have uncovered phenomena whose physical origins remain under investigation.[5−7,11] We aim to both clarify previous results and extend experimental studies of the diffusion of DNA molecules to greater confinement.

Balducci et al.[21] measured DNA diffusivity experimentally as a function h in nanoslits with $0.4 < R/h < 15$, where R is the DNA bulk radius of gyration. Although a transition from blob theory to reflecting rod theory has been observed by examining DNA relaxation times in nanochannels with square cross sections,[22] Balducci et al. found no such transition and determined that D scales more weakly with h than predicted by blob theory. Hsieh et al.[10] confirmed this weaker scaling for similar confinement but measured a systematic shift in D as compared to the results of Balducci et al.,[21] which they attributed to differences in the buffers used. Stein et al.[23] probed confinements up to $R/h < 7$ and concluded that blob theory correctly predicts the scaling of D with h in nanoslits. Lin et al.[24] also claimed agreement with blob theory for the scaling of D with h, having varied N for fixed h with $R/h < 14$.

Disagreement present in the experimental literature regarding the scaling of D with h also exists in simulation results. The Brownian dynamics simulation of Jendrejack et al.,[25] which included hydrodynamic interactions between DNA segments as well as between DNA and the channel, corroborated previous simulations by Harden and Doi:[26] both studies stated disagreement between their results and the predictions of blob theory for the scaling relationship between D and h in square channels. To help explain their conclusions, Jendrejack et al.[25] invoked a further length scale for polymer interactions with the confining channel boundary that prohibits blob theory scaling. In contrast, a comparable simulation,[27] as well as one using the lattice Boltzmann method,[28] obtained qualitative agreement with the predictions of blob theory in slit geometries. However, Hsieh et al.[10] claimed that closer inspection of these simulations revealed a slightly weaker dependence of D on h than that predicted by blob theory.

The scaling relationship between D and N has also been investigated and contains information regarding the effects of hydrodynamic interactions on DNA dynamics. The screening of hydrodynamic interactions over a distance equal to the smallest confining dimension is predicted by both blob and

* Corresponding author. E-mail: eas58@cornell.edu.
† Department of Physics.
‡ School of Applied and Engineering Physics.
§ These authors contributed equally.

10.1021/ma801313w CCC: $40.75
Published on Web 10/04/2008

reflecting rod theories and was first observed experimentally by Bakajin et al.[29] in 90 nm deep nanoslits. Balducci et al.[21] later determined that the influence of hydrodynamic interactions on DNA diffusion in nanoslits is negligible for depths slightly smaller than R.

Our results were obtained using single-molecule epifluorescence video microscopy to observe the free diffusion of individual 10 kbp, (1/2)λ, and λ DNA molecules in fused-silica nanoslits with depths between 541 and 24 nm. Taking R to be approximately 700 nm for λ DNA[21] and $R \propto N^{3/5}$ as stated by Flory,[30] we probed the dynamics of individual DNA molecules in nanoslits with $0.5 < R/h < 29$. By measuring D as separate functions of h and N, we tested the applicability of blob theory, observed whether a transition to reflecting rod theory is evident at nanoslit depths below the persistence length, and verified that hydrodynamic interactions remain screened in these systems. Our results may also indicate the lower depth limit for the use of our fused-silica nanoslits for analyzing the dynamics of highly confined DNA, where typical assumptions, such as neglect of surface roughness, become invalidated.

2. Theory

Arguments for the theoretical scaling of D with h and N are summarized by Balducci et al.[21] for blob and reflecting rod theories. In free solution, a DNA molecule undergoes a random self-avoiding walk (SAW) in three dimensions with an average size[30] $R \propto N^{3/5}$. When the DNA molecule, which has a persistence length, p, is confined moderately to a nanoslit such that $p \ll h \ll R$, the polymer may be modeled by a series of noninteracting spherical blobs, each of size h, undergoing a two-dimensional SAW.[18] Polymer segments within a blob do not feel the effects of confinement and continue to behave as in free solution. The number of monomers per blob scales as $h^{5/3}$, giving $Nh^{-5/3}$ blobs per polymer. If the DNA is confined further, such that $p \geq h$, the polymer segments within each blob begin to feel the effects of confinement, and the polymer is theorized to be described more accurately by a series of rods of length $l \propto p^{1/3}h^{2/3}$ that reflect off of the channel surfaces.[19,31] The number of rods per polymer is given by N/l. This length has been derived for channels with circular, square, and rectangular cross sections,[32,33] although uncertainties remain regarding polymer conformation in nanoslits whose widths are much larger than p.[33,34]

From Einstein's relation, D is inversely proportional to the viscous friction coefficient, ξ, of the DNA molecule, which in turn depends upon the DNA conformation in the confining nanoslit. In this way, measurements of the diffusion of DNA molecules contain information about the conformation of molecules experiencing various degrees of confinement. Both blob and reflecting rod theories assume that hydrodynamic interactions between polymer segments (blobs or rods) are absent, since these interactions are screened over the length scale imposed by the confining channel depth. In this case, the total value of ξ is given by the product of the number of polymer segments and the value of ξ for a single segment. Using estimates for ξ for a blob[15,18] and a rod,[35] we obtain the following expressions for D according to each theory:

$$\xi_{\text{blob}} \propto h \tag{1}$$

$$D_{\text{blob}} \propto (\xi_{\text{blob}} N_{\text{blob}})^{-1} \propto h^{2/3} N^{-1} \tag{2}$$

$$\xi_{\text{rod}} \propto l(\ln(h/d))^{-1} \tag{3}$$

$$D_{\text{rod}} \propto (\xi_{\text{rod}} N_{\text{rod}})^{-1} \propto \ln(h/d) N^{-1} \tag{4}$$

where d represents the diameter of a DNA molecule.

Expressions for D in both blob and rod theories contain an N^{-1} dependence that is also present in the Rouse model of unconfined Brownian motion of a polymer,[14] in which hydrodynamic interactions are neglected explicitly. Given that the number of polymer segments is linearly proportional to N for any h, and hydrodynamic interactions are assumed to be screened over a length that is independent of N, corroboration of Rouse scaling of D with N is expected for all nanoslit depths examined here.

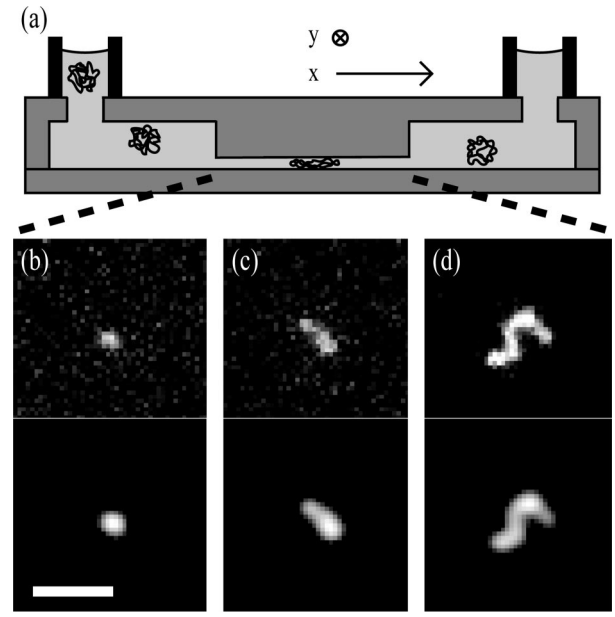

Figure 1. (a) Side-view schematic of a nanoslit device containing DNA molecules (not to scale). DNA molecules were loaded into a confining nanoslit from deeper regions on either side and were observed using epifluorescence video microscopy as they diffused freely. Raw and processed images of 10 kbp (b), (1/2)λ (c), and λ DNA (d) in a 24 nm deep nanoslit capture the DNA in relatively elongated conformations, accentuating size differences between the DNA lengths (scale bar: 5 μm). To facilitate comparison, contrast settings are identical for the raw and processed images, separately. The processed images have been convolved (section 3.D), in order to discriminate the boundary of the DNA molecule from background noise.

3. Experimental Materials and Methods

3.A. Device Fabrication and Design. Devices were fabricated from fused-silica wafers (Mark Optics), with specified root-mean-square surface roughness <0.5 nm, using two layers of contact photolithography and reactive ion etching (CHF_3/O_2). Most devices consisted of one 150 μm wide channel with a 1 mm long nanoslit and 1 cm long, approximately 0.5 μm deep region on either side of the nanoslit (Figure 1a). An access hole was created at each end of the device using microabrasive blasting. A wafer with 28 nm deep nanoslits was fabricated as part of an alternative device geometry, in which the nanoslit was 50 μm wide and 1 cm long. Device wafers were fusion bonded to 170 μm thick fused-silica wafers and annealed. Plastic reservoirs were attached using silicone adhesive.

Devices were characterized prior to bonding. Channel depths were determined using a Tencor P-10 surface profiler. Nanoslits were measured to be 541, 91, 45, 28, and 24 nm deep, with fractional errors of 1% or less for the three deepest nanoslits, approximately 4% for the 28 nm deep nanoslit, and approximately 7% for the 24 nm deep nanoslit. Eight nanometer deep nanoslit devices were also fabricated but collapsed during bonding and annealing.[8] Atomic force microscopy (AFM; Digitial Instruments Dimension 3000, Veeco Instruments Inc.) was used to determine surface roughness. AFM images were obtained in tapping mode with probes (TESP, Veeco Instruments, Inc.) specified to have a tip radius <10 nm and analyzed using DI Nanoscope software (Digital Instruments/Veeco). The root-mean-square surface rough-

ness averaged for the etched regions was similar to the average value for adjacent, unprocessed regions on all device wafers, excepting several features in each 25 μm^2 scan of the etched regions with heights between 10 and 20 nm. The exact widths of these features could not be determined, due to the limitations inherent in AFM measurements of very narrow topological aspects. Neither the frequency nor apparent shape of these spike-like features correlated with etch depth. However, the potential influence of these features on DNA diffusion increases with decreasing nanoslit depth, because the surface roughness occupies a larger percentage of the total nanoslit volume for smaller depths.

In order to obtain measurements of the bulk diffusion of DNA molecules, a poly(dimethylsiloxane) (PDMS) microfluidic device was constructed and contained a long, 50 μm wide and approximately 48 μm deep channel. PDMS (Sylgard 184, Dow Corning Corp.) was mixed at an elastomer to hardener ratio of approximately 10:1, poured over a silicon master that had been fabricated using reactive ion etching and treated with SigmaCote (Sigma-Aldrich), and cured at 60 °C for several hours. Large holes punched at either end of the channel through the PDMS served as reservoirs, and the device was bonded irreversibly using an oxygen plasma treatment to a 170 μm thick fused-silica wafer.

3.B. DNA Samples. The 10 kbp, (1/2)λ, and λ DNA (48.5 kbp) molecules (New England Biolabs) were diluted in 5× Tris−borate−EDTA (TBE) buffer (Sigma) and labeled at a 5:1 (base pair/dye molecule) ratio with YOYO-1 fluorescence dye (Invitrogen). (1/2)λ DNA was created using an XbaI (New England Biolabs) digestion, which produced DNA with lengths of 24 508 bp and 23 994 bp. Results of the λ DNA digestion were verified using an agarose gel separation.

3.C. Experimental Procedure. Molecules were observed using an inverted microscope (IX70, Olympus), 60× 1.45 NA oil immersion TIRFM coverslip-corrected objective (Olympus), broad spectrum light source (mercury arc lamp, Olympus, or X-Cite 120 PC, Exfo), filter cube set XF100 (Omega Optical Inc.), and Cascade 512b EMCCD (Photometrics). In-plane drift of the microscope stage was controlled using a precision microscope stage (ProScan II, Prior Scientific) with a 40 nm step size and correction for a drift of three steps. Data was collected using custom software written in Labview (National Instruments Corp.).

Devices were filled via capillarity with a filtered solution (all filters 0.1 μm pore size, Whatman) of 70% ethanol and 30% 18 MΩ water (Millipore). Before each experiment, devices were flushed using a dc voltage (PS325, Stanford Research Systems) applied for 1 h with filtered 5× TBE buffer containing 4% (v/v) β-mercaptoethanol (Sigma) that had been made immediately prior to the start of the experiment. This buffer contacting fused silica results in a Debye length[36] of <1 nm. After flushing, fluid in the reservoirs was replaced with fresh buffer, and a DNA solution was added carefully to a reservoir in order to minimize shearing of the sample. The total volume in each reservoir was 50 μL; equal volumes prevented pressure flow through the device. DNA concentrations in the reservoirs ranged from 0.03 to 0.2 μg/mL. DNA molecules were driven electrokinetically into the nanoslits using between 50 and 200 V applied via gold wires inserted into the reservoirs, which were covered to prevent evaporation. All experiments were performed at room temperature. The following procedure was followed to collect data from a single molecule: a molecule was identified approaching the nanoslit at least 20 μm away from the channel sidewalls; the shutter was closed to prevent photobleaching and photocleaving of the molecule; the molecule was driven at least 100 μm into the nanoslit; the electric field was switched off; the molecule was allowed to relax after having elongated upon entering the nanoslit; the shutter was opened; acquisition of video images was begun. The time allowed for the 10 kp, (1/2)λ, and λ DNA molecules to relax was at most 30 s and at least 5, 10, and 10 s, respectively.[10] The video exposure time was 40 ms. The electric field was pulsed immediately after data acquisition to verify that the molecule had not become adsorbed permanently onto a channel surface. Rarely, molecules became partially immobilized onto the channel surface or entered the nanoslit in an apparent knot, and these videos were discarded. After experiments, devices were flushed overnight with fresh buffer to remove all remaining DNA and stored with 18 MΩ water.

The PDMS microfluidic channel was used to measure the bulk diffusivity of λ DNA in the buffer. This device was filled and prepared identically to the fused-silica nanoslit devices, with an additional immersion of the PDMS device in buffer for 1 h immediately prior to use to prevent buffer absorption by the PDMS from influencing diffusion measurements. After DNA molecules were pressure-driven into the channel, a small Petri dish with a hole in the bottom was affixed upside-down using silicone sealant over the entire device. Additional buffer was introduced through the hole, and this allowed the device to be submerged completely under buffer during data acquisition, which prevented pressure-driven fluid flow through the channel.

3.D. Data Analysis. Images of the DNA molecules were analyzed using custom software written for MATLAB (The Mathworks). The *x*- and *y*-axes are defined to be along and perpendicular to the longitudinal axis of the nanoslit, respectively, and in the plane of the nanoslit (Figure 1a). Each frame was convolved with a kernel intended to reduce the background fluorescence and minimize the signal noise over a region appropriate for the spatial extent of a DNA molecule of a given length in a given nanoslit. This was implemented by subtracting a boxcar average from a Gaussian surface of revolution of half-width equal to one pixel (267 nm), which served to minimize digitization noise from the CCD without blurring the image.[37] All pixels with an intensity value below a threshold of approximately 33% of the maximum value were discarded. A DNA molecule was located by identifying the largest connected region of the remaining pixels.[38] Figure 1b−d depicts raw and processed images of individual 10 kbp, (1/2)λ, and λ DNA molecules in a 24 nm deep nanoslit acquired according to this algorithm.

The intensity-weighted center of mass of the molecule, $\mathbf{r}_{cm}$, for a given video frame at time t was calculated according to

$$\mathbf{r}_{cm}(t) = \frac{\sum \mathbf{r} I(\mathbf{r}, t)\, d\mathbf{r}}{\sum I(\mathbf{r}, t)\, d\mathbf{r}} \tag{5}$$

where the sum was taken over all pixels belonging to the molecule as determined above, and $I(\mathbf{r},t)$ represents the intensity at position $\mathbf{r}$. The results were not affected by the substitution of convolved intensity values for raw values, once the pixels comprising the DNA molecule had been located. For each nanoslit depth less than 100 nm and each DNA length, the center of mass position was tracked as a function of time over roughly 15 s for approximately 25 molecules. In the 541 nm deep nanoslit, an average of 10 molecules of each length were observed for approximately 15 s each. The center of mass displacement was computed for the *x*- and *y*-axes separately as a function of the time interval between frames.

The Einstein−Smoluchowsky equation relates a particle's Brownian motion to D according to

$$\langle \Delta x^2(t) \rangle + \langle \Delta y^2(t) \rangle = 4Dt \tag{6}$$

where brackets denote the average over many time intervals for a single molecule or over the displacement of multiple molecules for a given time interval. D (averaged over h) was measured from the slope of a linear fit to the mean square displacement, MSD, versus t for the *x*- and *y*-axes separately from the ensemble of molecules for each N and h (Figure 2a). These distributions were fit from 0.5 to 1.5 s, with data points every 40 ms, to extract D.[21] Error on the MSD for a given t was calculated by taking the standard deviation of the MSD divided by the square root of the number of displacements for that t. The χ^2 minimization fit to the plot of MSD versus t failed to take into account correlations between data points that resulted from the use of each molecule's trajectory to calculate the MSD for each t (up to 1.5 s). Consequently, the error of the fit was underestimated by a factor of approximately 1.55. This value was determined by sampling randomly from ensembles of model

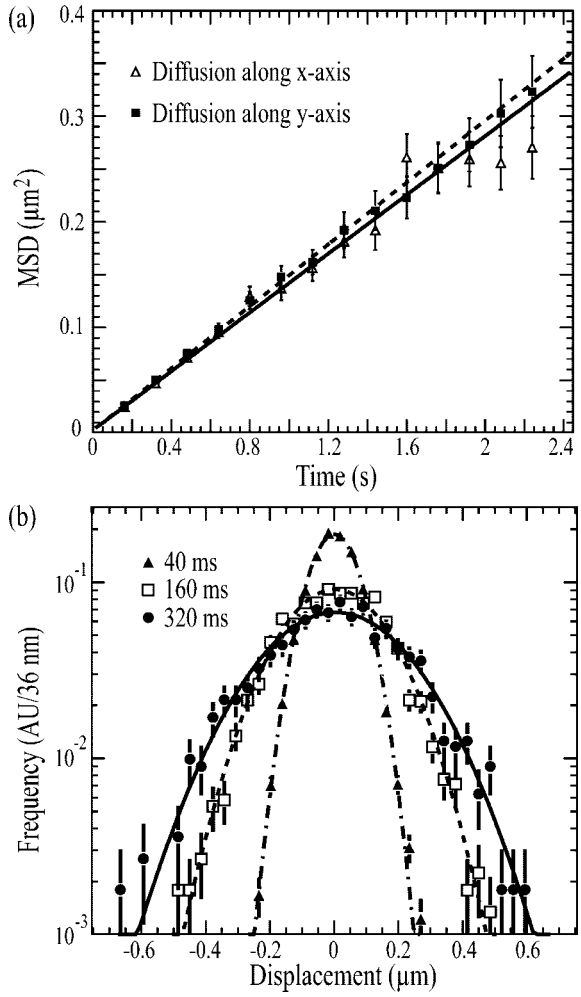

Figure 2. (a) MSD of λ DNA in a 90 nm slit for displacements along the *x*- (open triangle) and *y*-axes (solid square) as a function of time. The MSD was fit to a line between 0.5 and 1.5 s with data points every 40 ms to extract *D*, which was (0.068 ± 0.004) μm^2/s for λ DNA in this nanoslit. (b) Probability distributions with Gaussian fits for the displacement of λ DNA along the *y*-axis in a 90 nm slit after 40 (solid triangle), 160 (open square), and 320 (solid circle) ms. The plots have been normalized to the same number of events. The variance of these distributions provides an additional method for measuring the MSD as a function of time (ref 36).

diffusivity distributions and plotting the distribution of the difference between input and fit values of *D*, divided by the error returned from the fit. For uncorrelated data, this distribution should be a unit Gaussian with mean zero. The error on the fit to the experimental data was scaled to account for this bias. The measured diffusivity in the ensembles was consistent with the input value to within 0.1%, which is significantly more precise than the statistical uncertainty of the measurements of *D* in the nanoslits.

In general, the MSD increased linearly with time, and good agreement was found between MSD values calculated for both the *x*- and *y*-directions. The probability distribution of displacements for various elapsed times was examined, in order to ascertain whether appreciable fluid flow occurred through the nanoslits during measurements. Assuming no net fluid flow, *D* can also be measured from the variance of this distribution.[39] The resulting probability distributions were well-fit by a Gaussian function (Figure 2b), and the value of *D* calculated from the variance at a given elapsed time agreed well with the slope of the line fitted to the MSD data. However, significant disagreement was observed for *D* measured along the *x*- and *y*-axes in the 24 nm deep nanoslit.

Eliminating induced motion of DNA molecules in nanochannels can be difficult, and the mean of the displacement probability

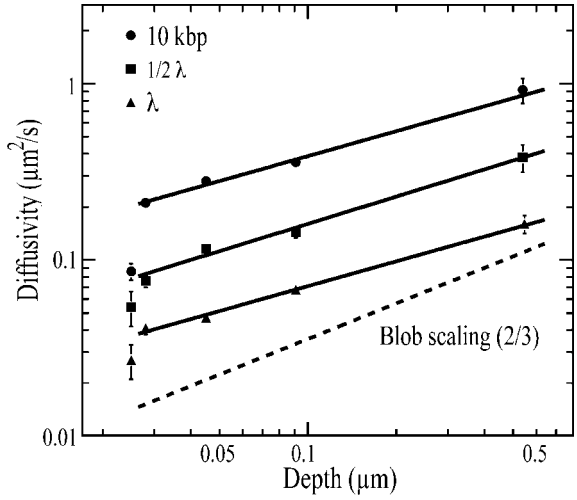

Figure 3. *D* vs *h* for 10 kbp (circle), (1/2)λ (square), and λ (triangle) DNA. Solid lines represent power-law fits to the data, excluding data from the 24 nm deep nanoslit. The slopes are 0.47 ± 0.05, 0.51 ± 0.06, and 0.47 ± 0.05 for the 10 kbp, (1/2)λ, and λ DNA, respectively, and agree well with previous experiments (refs 10 and 21) but disagree with the predictions of blob theory (shown as a dashed line). Data for the 24 nm nanoslit clearly do not follow the same scaling (section 4). Error bars for the 24 nm nanoslit represent half the difference between *D* obtained for displacements along the *x*- and *y*-axes, because this value is greater than the statistical error.

distribution for the *x*-axis was shifted linearly with time for some measurements, indicating fluid flow. This may have been caused by a small pressure drop due to uneven fluid levels in device reservoirs or a residual electrical potential drop across the nanoslit. In these cases, the product of *t* and the mean drift velocity, v_d, calculated from all molecules in the data set for a given *N* and *h* was subtracted from the displacement at each *t*, and *D* was recomputed. The difference between the nominal and corrected values for *D* lay well within the statistical error on the nominal value. In other words, $(Dt)^{1/2} \gg v_d t$ for all *t* used to calculate *D*.

In order to calibrate the procedure for data analysis, the value of *D* for unconfined λ DNA molecules was measured in a PDMS microchannel prepared as described in section 3.C. Approximately 25 molecules were observed for an average of 5 s each, until they diffused out of the objective's depth of field. The measured value of *D* was (0.49 ± 0.04) μm^2/s, which is in good agreement with previous measurements.[21,27,40]

4. Results and Discussion

The gap-averaged diffusivity of DNA molecules of different lengths as a function of nanoslit depth is plotted in Figure 3 for DNA molecules and nanoslits with $0.5 < R/h < 29$. Power-law fits to the data are shown. Excluding data measured in the 24 nm deep nanoslit, *D* scaled with *h* according to $D \propto h^{\alpha}$, where α was 0.47 ± 0.05, 0.51 ± 0.06, and 0.47 ± 0.05 for 10 kbp, (1/2)λ, and λ DNA, respectively. This scaling disagreed with the exponent value of two-thirds predicted by blob theory, which was formulated originally for polymers confined such that $h \gg p$. This condition was invalid for DNA molecules in four of the five nanoslits used here. However, the measured scaling of *D* agrees with previous experiments[10,21] that investigated the range of $0.4 < R/h < 15$, as well as with a Brownian dynamics−hydrodynamic simulation of DNA in microchannels[25] that extended to $R/h \sim 10$. Additionally, the discrepancy with blob theory predictions may be attributed to partial-draining blobs resulting from the relatively small number of persistence length segments per blob in nanoslits with the depths used here.[10,41] Our results show that a power law with an exponent of approximately one-half describes the scaling relationship between *D* and *h* over a large range of DNA confinement that

extends to nanoslits with $h < p$. Within the precision of our measurements, no significant statistical difference was evident in the scaling of D with h for different N. However, small differences have been measured, where the authors questioned whether blobs of DNA contained a sufficient number of monomers at nanoslit depths on the order of a persistent length to follow the excluded-volume swelling expected by blob theory.[21] Quantitative comparison was difficult between the observed scaling of D with h and that predicted by reflecting rod theory (eq 4) for the nanoslits in our study with depths less than the persistence length of DNA, because only three nanoslits satisfied the condition $h < p$, and the scaling normalization is unknown. Nevertheless, a power-law spectrum provided a good description of D over the full range of confinement investigated here (excluding results from the 24 nm deep nanoslit), which extended well into the expected reflecting rod regime[22] and agreed with the work of Balducci et al.[21]

Data from the 24 nm deep nanoslit were excluded from the analysis, because D measured for diffusion along the x- and y-axes did not agree. In order to better understand this result, D of λ DNA molecules was measured in separate experiments using two 24 nm nanoslits fabricated on the same wafer. The wafer orientation with respect to the camera and optics was rotated by 90° between these experiments, in order to rule out potential orientation effects produced by the optical system. For both experiments, the observed average diffusivity was 1.7 ± 0.2 times larger along the x-axis than the y-axis. During electrokinetic injection of DNA molecules into a nanoslit prior to observation (section 3.C), molecules were stretched along the x-axis due to a combination of the electric field gradient and entropic effects[2] at the nanoslit entrance. The rotational relaxation time for λ DNA in a 24 nm nanoslit is approximately 5 s,[10] and DNA molecules were allowed at least 10 s between removal of the electric field and recording data. This should have allowed the DNA molecules to return to an equilibrium extension and assume a random orientation. Nevertheless, the orientation of the DNA molecules remained highly correlated with their initial orientation along the x-axis during the entire analysis time of approximately 15 s. Orientation was determined according to the method described by Maier and Radler,[42] which used the second moment of the fluorescence intensity distribution. Examination of the probability distribution function for displacement at various elapsed times did not indicate that the molecules experienced a drift velocity. D of $(1/2)\lambda$ DNA molecules was also 1.8 ± 0.2 times larger along the x-axis than the y-axis in the 24 nm deep nanoslit, and the discrepancy was a factor of 1.1 ± 0.1 for the 10 kb DNA. Interestingly, ξ for a rod moving perpendicular to its major axis is approximately twice as large as ξ for motion parallel to its major axis.[43]

To investigate further, a computer-controlled shutter was fitted to the camera, and 90 s videos of λ DNA in a 24 nm deep nanoslit were taken with 40 ms exposures and 160 ms shuttered periods between exposures. Use of the shutter limited photodegradation of the dye and DNA molecules, allowing for much longer observation times. The discrepancy persisted between D values measured along the x- and y-axes.

The significant disparity between D measured along the x- and y-axis in the 24 nm nanoslit is not yet understood fully, although interactions between the DNA and nanoslit surface roughness, such as the spikelike surface features (section 3.A), may have played a role. Although no molecules included in the analysis had become permanently adsorbed onto a channel surface, video images indicated that portions of some molecules may have interacted transiently with the channel surface for a significant time during diffusion in the 24 nm deep nanoslits. Although it is unknown why the disparity was evident in the 24 nm but not 28 nm deep nanoslit, differences in D may be attributable to material or fabrication variations between the wafers constituting these devices. Consequently, we excluded data obtained in the 24 nm deep nanoslits from our determination of the power-law exponents.

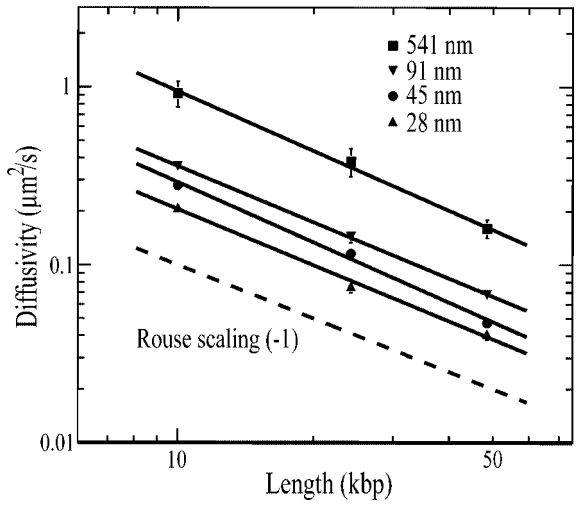

Figure 4. D vs N for 541 (square), 91 (inverted triangle), 45 (circle), and 28 (triangle) nm deep nanoslits. Solid lines represent power-law fits to the data. The slopes yielded by these fits are -1.12 ± 0.12, -1.05 ± 0.06, -1.12 ± 0.06, and -1.05 ± 0.07, respectively. These values are in good agreement with the prediction of Rouse dynamics (shown as a dashed line) indicating hydrodynamic screening between the polymer segments.

We also note that D measured along both dimensions in the 24 nm deep nanoslit was significantly smaller than the value of D predicted by reflecting rod theory, normalized to results from the 45 nm deep nanoslit (data not shown).

The gap-averaged diffusivity of DNA molecules was also plotted as a function of N (Figure 4) for $0.5 < R/h < 25$. Power-law fits yielded slopes of -1.12 ± 0.12, -1.05 ± 0.06, -1.12 ± 0.06, and -1.05 ± 0.07 for molecules in the 541, 91, 45, and 28 nm deep nanoslits, respectively. These scaling exponents were in accordance with the relationship $D \propto N^{-1}$ from Rouse dynamics. However, all measured exponents were systematically larger than this prediction. Our results agree well with previous experimental measurements[10,21,24] that found negligible effects due to hydrodynamic interactions for $R \sim h$. The measurements presented here extend these results to more highly confined DNA molecules, where both blob and reflecting rod theories yield identical predictions of $D \propto N^{-1}$. Despite our reservations regarding data taken in the 24 nm deep nanoslit, this scaling result also holds for D measured separately along x- and y-axes in the 24 nm deep nanoslit.

5. Conclusions

We observed the free diffusion of individual 10 kbp, $(1/2)\lambda$, and λ DNA molecules in fused-silica nanoslits with depths between 541 and 24 nm. Scaling of the diffusivity with nanoslit depth was in good agreement with previous studies and disagreed with the value predicted by blob theory. A clear transition from blob theory to reflecting rod theory was not identified, because a single power-law exponent fit the data for all DNA lengths and nanoslit depths from 541 to 28 nm. The expected Rouse scaling of diffusivity with DNA length was observed for all nanoslit depths, indicating screening of hydrodynamic interactions. Results from the shallowest nanoslit were excluded from these fits to determine scaling exponents, due to significant differences between the diffusivities measured along the x- and y-axes, the origin of which remains poorly understood. The measurements made in the 24 nm deep nanoslit provide an example of the potential impact that the nanoscale

material properties of a nanofluidic device can have on measuring the behavior of individual molecules forced into close contact with channel surfaces. With the shrinking dimensions of fluidic devices used for biomolecular manipulation and analysis, including nanoslits, knowledge of the fundamental behavior of highly confined polymer-like biomolecules is essential to advancing the utility of these structures.

Acknowledgment. The work was supported in part by the Nanobiotechnology Center (NBTC), an STC Program of the National Science Foundation under Agreement No. ECS-9876771. Fabrication was performed at the Cornell Nanoscale Facility, a member of the National Nanotechnology Infrastructure Network, and the Cornell Center for Materials Research, both supported by the National Science Foundation. The authors thank Christian Reccius for use of his Labview program for video acquisition, Leon Bellan for assistance performing atomic force microscopy, Karen Jarvis for assistance with (1/2)λ DNA preparation, and Samuel Stavis for review.

References and Notes

(1) Fu, J. P.; Schoch, R. B.; Stevens, A. L.; Tannenbaum, S. R.; Han, J. Y. *Nat. Nanotechnol.* **2007**, *2*, 121–128.
(2) Han, J.; Craighead, H. G. *Science* **2000**, *288*, 1026–1029.
(3) Wang, Y. C.; Stevens, A. L.; Han, J. Y. *Anal. Chem.* **2005**, *77*, 4293–4299.
(4) Lee, J. H.; Chung, S.; Kim, S. J.; Han, J. Y. *Anal. Chem.* **2007**, *79*, 6868–6873.
(5) Salieb-Beugelaar, G. B.; Teapal, J.; van Nieukasteele, J.; Wijnperle, D.; Tegenfeldt, J. O.; Lisdat, F.; van den Berg, A.; Eijkel, J. C. T. *Nano Lett.* **2008**, *8*, 1785–1790.
(6) Cross, J. D.; Strychalski, E. A.; Craighead, H. G. *J. Appl. Phys.* **2007**, 102.
(7) Krishnan, M.; Monch, I.; Schwille, P. *Nano Lett.* **2007**, *7*, 1270–1275.
(8) Strychalski, E. A.; Stavis, S. M.; Craighead, H. G. *Nanotechnology* **2008**, *19*.
(9) Hsieh, C.-C.; Balducci, A.; Doyle, P. S. *Nano Lett.* **2008**, *8*, 1683–1688.
(10) Hsieh, C. C.; Balducci, A.; Doyle, P. S. *Macromolecules* **2007**, *40*, 5196–5205.
(11) Pennathur, S.; Baldessari, F.; Santiago, J. G.; Kattah, M. G.; Steinman, J. B.; Utz, P. J. *Anal. Chem.* **2007**, *79*, 8316–8322.
(12) Jo, K.; Dhingra, D. M.; Odijk, T.; de.Pablo, J. J.; Graham, M. D.; Runnheim, R.; Forrest, D.; Schwartz, D. C. *Proc. Natl. Acad. Sci. U.S.A* **2007**, *104*, 2673–2678.
(13) Stavis, S. M.; Corgie, S. C.; Cipriany, B. R.; Craighead, H. G. *Biomicrofluidics* **2007**, *1*.
(14) Doi, M. *Introduction to Polymer Physics*; Clarendon Press: Oxford, 1992; p 75.
(15) Brochard, F.; Degennes, P. G. *J. Chem. Phys.* **1977**, *67*, 52–56.
(16) Neto, C.; Evans, D. R.; Bonaccurso, E.; Butt, H. J.; Craig, V. S. J. *Rep. Prog. Phys.* **2005**, *68*, 2859–2897.
(17) Brochard, F. *J. Phys.* **1977**, *38*, 1285–1291.
(18) Daoud, M.; Degennes, P. G. *J. Phys.* **1977**, *38*, 85–93.
(19) Odijk, T. *Macromolecules* **1983**, *16*, 1340–1344.
(20) Bouchiat, C.; Wang, M. D.; Allemand, J. F.; Strick, T.; Block, S. M.; Croquette, V. *Biophys. J.* **1999**, *76*, 409–413.
(21) Balducci, A.; Mao, P.; Han, J. Y.; Doyle, P. S. *Macromolecules* **2006**, *39*, 6273–6281.
(22) Reisner, W.; Morton, K. J.; Riehn, R.; Wang, Y. M.; Yu, Z.; Rosen, M.; Sturm, J. C.; Chou, S. Y.; Frey, E.; Austin, R. H. *Phys. Rev. Lett.* **2005**, *94*, 196101.
(23) Stein, D.; van der Heyden, F. H. J.; Koopmans, W. J. A.; Dekker, C. *Proc. Natl. Acad. Sci. U.S.A.* **2006**, *103*, 15853–15858.
(24) Lin, P.-K.; Fu, C.-C.; Chen, Y. L.; Chen, Y.-R.; Wei, P.-K.; Kuan, C. H.; Fann, W. S. *Phys. Rev. E* **2007**, *76*, 011806.
(25) Jendrejack, R. M.; Schwartz, D. C.; Graham, M. D.; de Pablo, J. J. *J. Chem. Phys.* **2003**, *119*, 1165–1173.
(26) Harden, J. L.; Doi, M. *J. Phys. Chem.* **1992**, *96*, 4046–4052.
(27) Chen, Y. L.; Graham, M. D.; de Pablo, J. J.; Randall, G. C.; Gupta, M.; Doyle, P. S. *Phys. Rev. E* **2004**, *70*.
(28) Usta, O. B.; Anthony, J. C. L.; Jason, E. B. *J. Chem. Phys.* **2005**, *122*, 094902.
(29) Bakajin, O. B.; Duke, T. A. J.; Chou, C. F.; Chan, S. S.; Austin, R. H.; Cox, E. C. *Phys. Rev. Lett.* **1998**, *80*, 2737–2740.
(30) Flory, P. J. *J. Chem. Phys.* **1949**, *17*, 303–310.
(31) Choi, M. C.; Santangelo, C. D.; Pelletier, O.; Kim, J. H.; Kwon, S. Y.; Wen, Z.; Li, Y.; Pincus, P. A.; Safinya, C. R.; Kim, M. W. *Macromolecules* **2005**, *38*, 9882–9884.
(32) Turban, L. *J. Phys.* **1984**, *45*, 347–353.
(33) Odijk, T. *J. Chem. Phys.* **2006**, *125*.
(34) Reisner, W.; Beech, J. P.; Larsen, N. B.; Flyvbjerg, H.; Kristensen, A.; Tegenfeldt, J. O. *Phys. Rev. Lett.* **2007**, *99*.
(35) Morse, D. C. *Macromolecules* **1998**, *31*, 7044–7067.
(36) Russel, W. B.; Saville, D. A.; Schowalter, W. R. *Colloidal Dispersions*; Cambridge University Press: Cambridge, 1989; p 102.
(37) Crocker, J. C.; Grier, D. G. *J. Colloid Interface Sci.* **1996**, *179*, 298.
(38) Sedgewick, R. *Algorithms in C*, 3rd ed.; Addison-Wesley: Reading, MA, 1998; pp 11−20.
(39) Russel, W. B.; Saville, D. A.; Schowalter, W. R. *Colloidal Dispersions*; Cambridge University Press: Cambridge, 1989; p 70.
(40) Smith, D. E.; Perkins, T. T.; Chu, S. *Macromolecules* **1996**, *29*, 1372–1373.
(41) Zhang, C.; Zhang, F.; van Kan, J. A.; van der Maarel, J. R. C. *J. Chem. Phys.* **2008**, *128*.
(42) Maier, B.; Radler, J. O. *Phys. Rev. Lett.* **1999**, *82*, 1911–1914.
(43) Kenward, M.; Slater, G. W. *Eur. Phys. J. E* **2004**, *14*, 55–65.

MA801313W